

*Chapter 4***COUPLED DYNAMICS OF TWO SIDE-BY-SIDE INVERTED
FLAGS**

Cecilia Huertas-Cerdeira, Boyu Fan, and Morteza Gharib. Coupled motion of two side-by-side inverted flags. *Journal of Fluids and Structures* 46:527–535,2018.

While chapters 2 and 3 aim to improve our understanding of the dynamics of a single inverted flag, energy harvesting devices do not typically consist of an isolated flag, but of an array of them. Understanding the interaction between flags is essential to predicting the energy harvesting performance of the system. Indeed, arrangement optimization is a full field of study in the development of traditional turbine wind farms (Samorani, 2013). It is particularly relevant, however, in turbines that rely on vortex dynamics to function, such as the inverted flag, because vortex wakes can interact strongly when in proximity.

The canonical problem studied in the fields of vortex shedding and vortex induced vibrations is that of a circular cylinder (for a review, see Williamson and Govardhan (2004)). The interaction between multiple cylinders placed in different arrangements has been reported extensively in the literature. In particular, interesting wake dynamics have been shown to arise when two fixed stationary cylinders are immersed side-by-side in a flow (Zdravkovich (2003) and references therein). Depending on the separation between them, they have been shown to generate either a single vortex street, two wakes of different widths that present a bi-stable gap flow, two equal and synchronized wakes or two completely uncoupled wakes. In the case of cylinders that are flexible or allowed to move the coupling of the wakes can result in the coupling of the motion of the cylinders (Huera-Huarte and Gharib, 2011; Liu et al., 2001; Zdravkovich, 1985; Zhou et al., 2001).

Similarly, two conventional flags placed side-by-side in a flow have been shown to interact. Zhang et al. (2000) experimentally studied the motion of two side-by-side filaments immersed in a soap film and observed both an in-phase flapping mode for small flag separations and an anti-phase flapping mode for larger flag distances. The anti-phase mode was observed to oscillate with frequencies 35% higher than those of the in-phase mode. As the distance was further increased, the interaction

weakened and the flags moved independently. Analogous results were obtained in numerical simulations by Zhu and Peskin (2003) and Farnell et al. (2004). Farnell et al. (2004), Si-Ying et al. (2013) and Sun et al. (2016) observed, in addition to the in-phase and out of phase modes, the existence of a transition mode where the frequencies of both motions co-exist. A different transition mode was reported by Jia et al. (2007), who observed a region where in-phase and out-of phase flapping alternate randomly. In addition to two equal filaments, Jia et al. (2007) studied the motion of two side-by-side filaments whose length varied by a factor of two and observed synchronization with a scattering of the phase around the 0 and π values.

These interactions with neighboring flags and their vortex streets can cause variations in the forces experienced by the flags. Many natural organisms exploit the vortex street of neighboring bodies to enhance their performance; an example is schooling fish. Changes in position and phase between the swimming motion of adjacent fish can drastically change the effect of schooling (Weihs, 1973). Inspired by this behavior, optimal arrangements of vertical axis wind turbines have been shown to increase energy extraction in wind farms (Whittlesey et al., 2010). Dong et al. (2016) showed that placing two flags side-by-side can produce increased energy extraction efficiency in a potential energy harvesting mechanism. It is expected that inverted flags will show a similar behavior, and placing several flags in close proximity may enhance their energy harvesting capabilities.

In this chapter, the coupling of the motion of two inverted flags in a side-by-side arrangement is investigated experimentally. Because the amplitudes of oscillation of the inverted flag vary greatly between the different regimes of motion (straight, flapping and deflected), the effective cross-sectional area of the flag undergoes significant changes between them. This causes the synchronization in the motion of the flags to occur at very different flag separations for the different regimes. In this study we have focused on distances at which the flags never collide ($1.7 < T/L < 5.4$), which are pertinent to the coupling of the vortex induced vibrations of the flags in the flapping and deflected regimes. Here, T corresponds to the cross-flow distance between flags and L the flag length (figure 4.1). The non-dimensional parameter \tilde{T} will be used throughout this chapter and is defined by

$$\tilde{T} = \frac{T}{L}$$

The flags will be labeled left flag and right flag, corresponding to their position

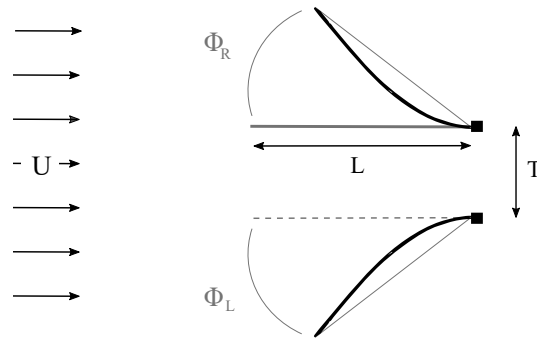


Figure 4.1: Top view of the side-by-side inverted flag arrangement and parameters employed for its characterization.

when the observer is located downstream of the flags and looking upstream, as represented in figure 4.1. The first series of experiments was conducted with two flags that had equal height (H , out of the paper) and length, L (flag 12 in table 1.3). In the second series, the height of both flags, H , and the length of one of the flags, L_0 , were maintained constant, while the length of the second flag, L , was varied (flags 13 - 22 in table 1.3).

4.1 Results

Flags of equal dimensions

The three main dynamic regimes present in the motion of a single flag (straight, flapping and deflected) as well as the chaotic motion described by Sader et al. (2016a) persist in the two flag system. For the distances \tilde{T} considered in this study and at low flow speeds (straight regime, figure 4.2a), the flags oscillate with small amplitude relative to the flag separation and no coupling occurs. As the wind speed is increased, the flag motion reaches angular amplitudes greater than 10 degrees, giving rise to periodic vortex shedding and flapping (Sader et al., 2016a). The lower critical wind speed, κ_{lower} , at which the flapping motion is onset was not observed to vary with the presence of the second flag. This is consistent with the onset of flapping occurring through an initial divergence instability that is dependent on the aerodynamic lift coefficient at small angles (Sader et al., 2016a). It is to be expected, however, that variations in the critical wind speed as well as synchronization in the straight regime will occur at flag separations smaller than those considered in this study.

In the flapping regime (figure 4.2b) the flags interact strongly. An increase in the angular amplitude of flapping of up to 36% was observed for the two-flag system with

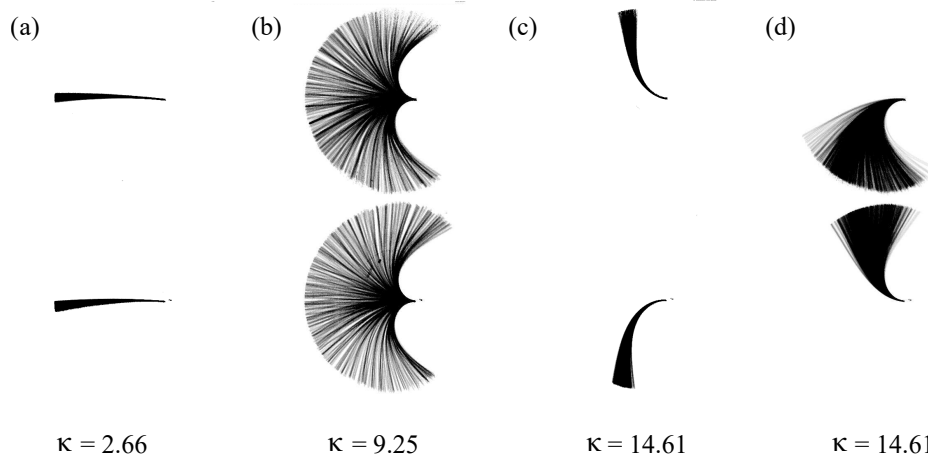


Figure 4.2: Stroboscopic progressions of the motion of the two-flag system showing the (a) straight regime, (b) flapping regime, (c) deflected regime in the outside-deflected configuration and (d) deflected regime in the inside-deflected configuration

respect to the single flag. Figure 4.3 shows the peak-to-peak amplitude of motion, averaged between the right and left flags, for varying separation distances. As the distance between flags is increased the gain in amplitude becomes less prominent, saturating at the single flag value for $\tilde{T} > 3.2$. This increase in amplitude is asymmetrical; as is evident from the stroboscopic progressions in figure 4.2b, the flags sweep a larger angle towards the interior (center) of the system. Small increases in frequency, up to 13%, were also observed at the smallest separations for the initial stages of the flapping regime. Increases both in the amplitude and frequency of flapping suggest that the energy available for harvesting in the two flag system is higher than that of the single flag.

Five different modes of flapping are present in the side-by-side inverted flag system. The angle ϕ of both flags as a function of time and the corresponding phase diagrams have been plotted in figure 4.4 for each of the modes. The phase diagrams have been colored to represent time: initially the curve is red and turns into blue as time advances. The modes include both an anti-phase regime (figure 4.4a), where the flags flap symmetrically, and an in-phase regime (figure 4.4b), where the flags flap anti-symmetrically. Staggered flapping, where the phase between flags is constant and between 0 and π , can also occur (figure 4.4c). In the alternating mode (figure 4.4d) the flags switch intermittently between two or more of the in-phase, anti-phase and staggered motions. This mode differs from the decoupled mode (figure 4.4e), where no coupling occurs, in the fact that the flags spend significantly more time

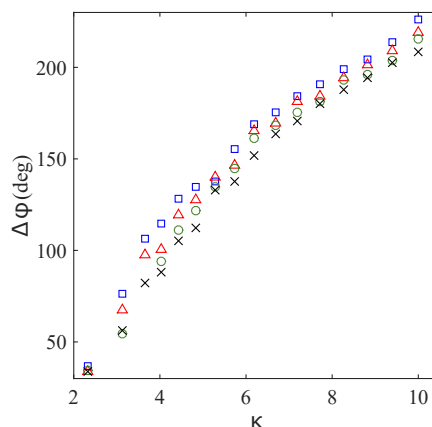


Figure 4.3: Peak-to-peak angular amplitude of motion, $\Delta\phi$, in the flapping regime for a single flag (\times) and two flags separated by $\tilde{T} = 2$ (\square), $\tilde{T} = 2.4$ (\triangle) and $\tilde{T} = 2.8$ (\circ). Represented values are the average of left and right flags.

in-phase, anti-phase and staggered than they do transitioning between the motions.

Because two identical flags have equal flapping frequency, they may appear to be flapping in-phase, anti-phase or staggered even if they are not interacting with each other. Therefore, in-phase, anti-phase or staggered modes have only been considered here when they constitute a steady state after starting from a different initial condition (see, for example, the phase diagram of staggered mode in figure 4.4c). In the current experiments, small variations in initial curvature, dimensions and angle of attack caused the frequencies of the right and left flags to differ, and therefore the phase between flags was observed to constantly change in the decoupled mode (figure 4.4e).

The relationship between wind speed, flag separation and flapping mode is summarized in figure 4.5. For small separations ($\tilde{T} < 3.5$), the flags were observed to flap mainly in the anti-phase mode. For the same range of velocities an in-phase motion can also occur. However, the anti-phase mode is energetically favorable and any staggered initial conditions or perturbations in the in-phase mode will lead to anti-phase flapping. As the distance between flags is increased, the range of velocities for which this predominantly anti-phase flapping is present decreases, giving rise to the staggered, in-phase and alternating modes. These appear for the higher wind speeds in the flapping range, while the anti-phase mode remains for the lower velocities. The distribution of staggered, in-phase and alternating modes for the different wind speeds and separation distances is not clearly defined. This

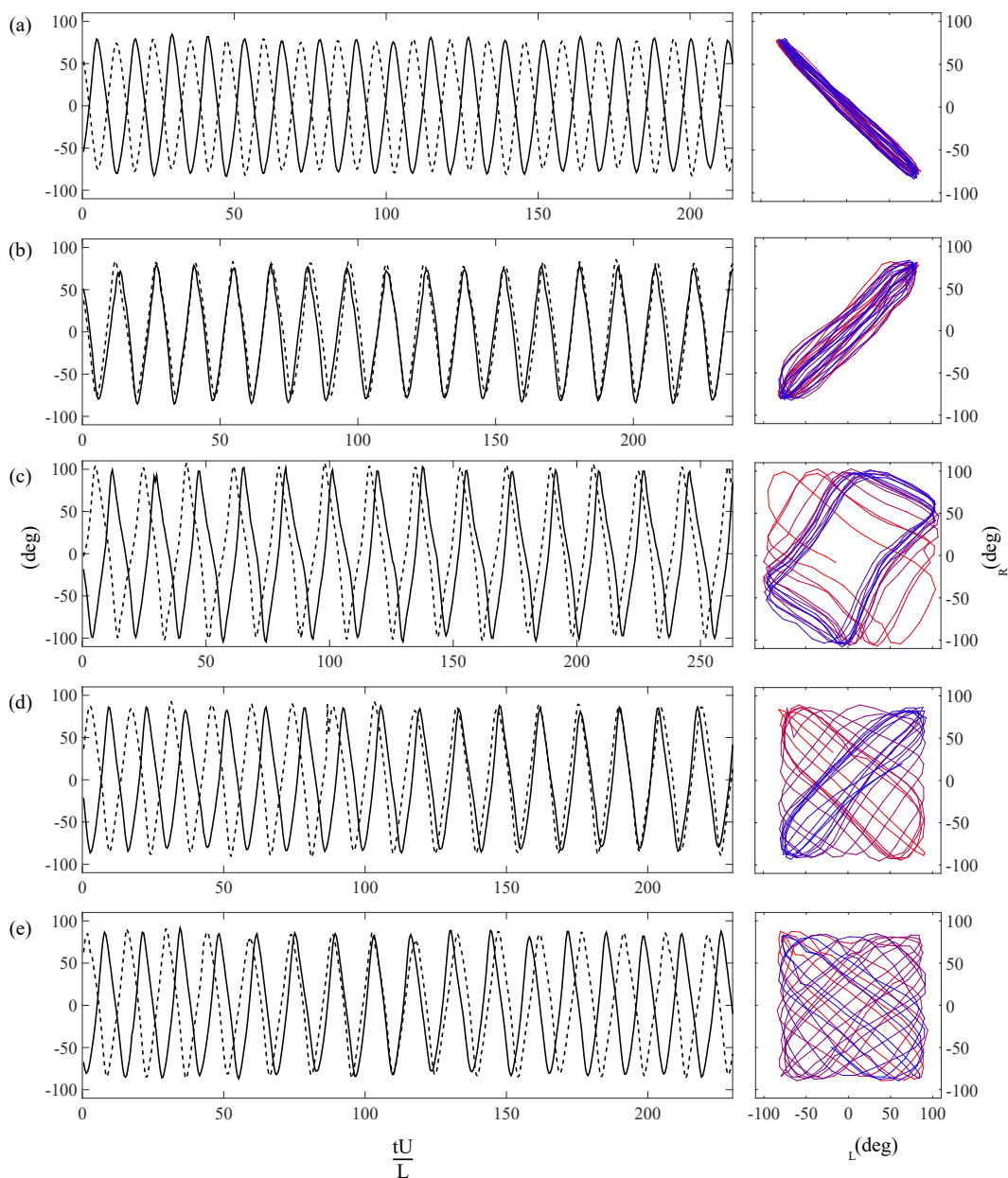


Figure 4.4: Time history of the angle ϕ for the left flag (solid line) and right flag (dashed line) on the left and phase diagram on the right for (a) anti-phase, (b) in-phase, (c) staggered (d) alternating and (e) decoupled modes. Phase diagrams have been colored to represent time, with the curve being initially red and shifting to blue as time advances

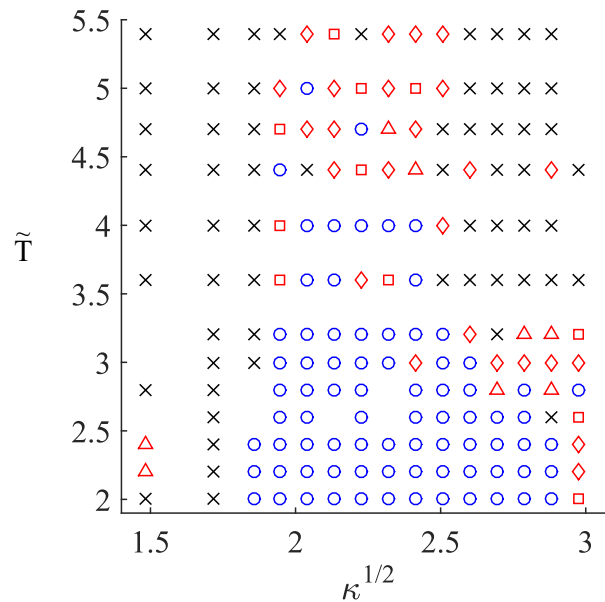


Figure 4.5: Flapping modes as a function of the dimensionless wind speed, $\sqrt{\kappa}$ and flag separation, \tilde{T} : (x) decoupled, (o) anti-phase, (Δ) in-phase, (\square) staggered and (\diamond) alternating. Not all possible modes are represented in this figure.

suggests that as the anti-phase flapping becomes less energetically favorable several modes are possible, with different initial conditions giving rise to different modes and perturbations causing the flags to switch from one mode to the other. At a distance of $\tilde{T} = 5$, the predominantly anti-phase flapping fully disappears. Finally, for large separation distances and high wind speeds the flags enter the decoupled regime, flapping uncoupled.

As wind speed is increased, the chaotic regime emerges. No synchronization was observed between the flags in this regime (see figure 4.6a). For wind speeds over a critical value the flags enter the deflected regime. No clear variations in the critical transition speed from the flapping to the deflected regimes have been observed for the two-flag system with respect to a single flag. For flow speeds immediately over the transition speed the flags deflect towards the outside region, independently of the initial condition (as depicted in figure 4.2c). The oscillating motion of the flags around this outside deflected position is independent, and therefore the flags only interact with each other at the initial stages, when they repel and force the outside deflected position. As flow speed is increased, however, the high fluid damping prevents the flags from changing side and inside (figure 4.2d), outside and asymmetric (one flag inside and one outside) deflected states are possible

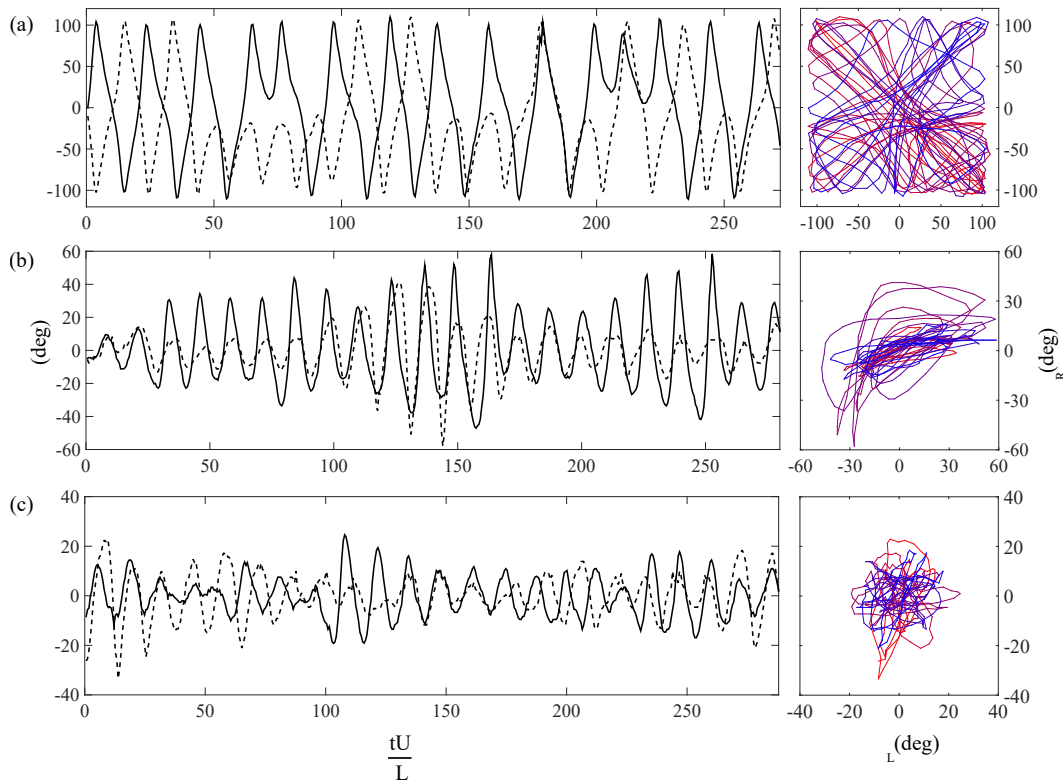


Figure 4.6: Time history of the angle ϕ for the left flag (solid line) and right flag (dashed line) on the left and phase diagram on the right for (a) chaotic, (b) inside-deflected in-phase and (c) inside-deflected decoupled. Phase diagrams have been colored to represent time, with the curve being initially red and shifting to blue as time advances. For the deflected states (b) and (c) the average has been subtracted.

depending on the initial conditions. There is, again, no coupling between outside or asymmetrically deflected flags. However, inside-deflected flags can synchronize in-phase when considering oscillations around the deflected equilibrium (figure 4.6b). As speed is further increased synchronization ceases (figure 4.6c).

Flags with different lengths

Flags that are equal in size have the same vortex shedding frequency, allowing for synchronization of the vortex streets and therefore of the motion of the flags. For flags of different lengths, on the other hand, the vortex shedding frequencies will not be equal. If these frequencies are sufficiently close, the vortex streets can still lock and synchronization will occur. Synchronization will cease, however, for flags that have significantly different lengths and therefore vortex shedding and natural frequencies. To study the effect of the relative length of the flags, a number of tests were performed in which the left flag was kept at a constant length, $L_0 = 0.1 m$,

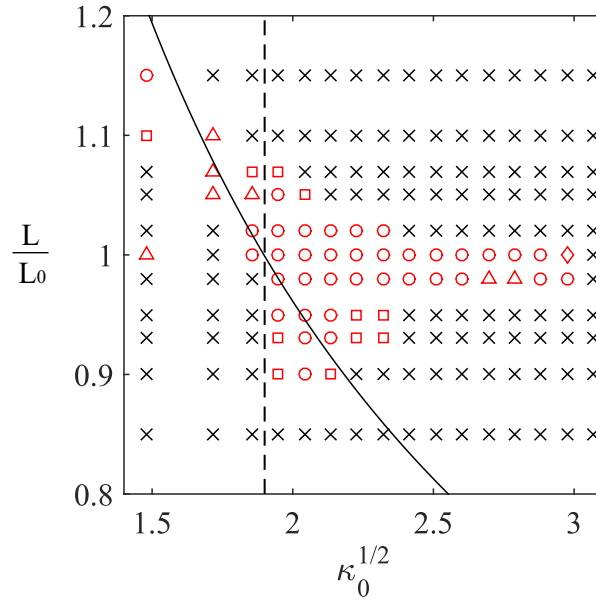


Figure 4.7: Flapping modes as a function of the dimensionless wind speed, $\sqrt{\kappa_0}$ and the flag length ratio, (L/L_0) : (\times) decoupled, (\circ) anti-phase, (Δ) in-phase, (\square) staggered and (\diamond) alternating. The distance between flags is constant ($T/L_0 = 2.4$). Lines represent the critical value of $\sqrt{\kappa_0}$ at which a single flag of length L_0 (dashed) and L (solid) enter the flapping regime.

while the length of the right flag, L , was varied. The distance between flags was maintained constant at $T/L_0 = 2.4$. The results are plotted in figure 4.7, where the length used for the dimensionless variable κ_0 is that of the left constant flag ($L_0 = 0.1 \text{ m}$).

For flags of the same length the results are equal to those reported in Section 4.1. The flags synchronize anti-phase for most of the velocities in the flapping range, although staggered modes are also present. As L is decreased, the range of velocities at which the flags synchronize decreases; at $L/L_0 \leq 0.85$ synchronization ceases to occur. Simultaneously, the anti-phase mode becomes less predominant, with the staggered mode being more prevalent. Similarly, as L is increased from the $L/L_0 = 1$ value, the range of wind speeds at which the flags synchronize decreases and the anti-phase mode vanishes in favor of in-phase and staggered motions.

Because the variations in aspect ratio are small, the critical value of κ at which both flags enter the flapping regime is approximately equal. Due to the difference in length, however, this corresponds to different values of the dimensional wind speed, meaning that there is a range of wind speeds at which the longer flag is in the flapping

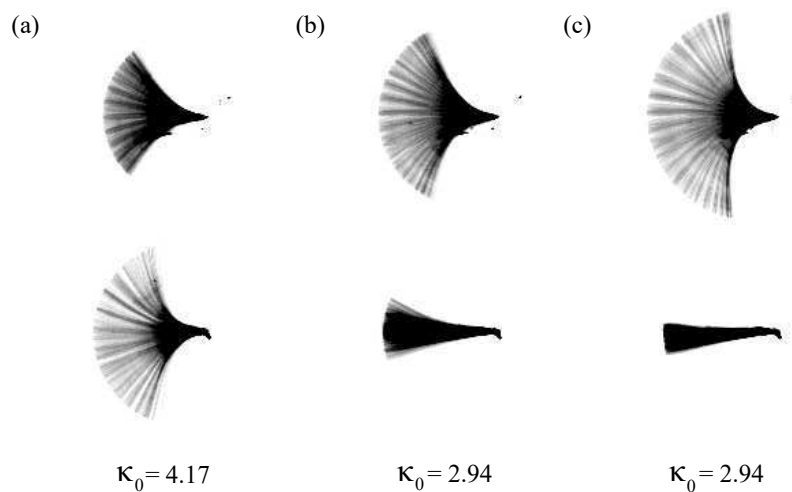


Figure 4.8: Stroboscopic progressions of the motion of two inverted flags of different lengths at a constant separation $T/L_0 = 2.4$, showing (a) the long flag inducing a flapping motion on the short flag ($L/L_0 = 0.9$), (b) the long flag inducing an oscillating motion on the short flag ($L/L_0 = 1.05$) and (c) the long flag flapping and the short flag oscillating uncoupled ($L/L_0 = 1.15$). The flag of constant length $L_0 = 0.1$ m is depicted at the bottom.

regime while the shorter one is in the straight regime. To identify these regions, the lines corresponding to the critical dimensionless velocity $\kappa_0 = \kappa_{lower}$ for each of the flags, as given by equation (2.15) in Sader et al. (2016b), have been plotted in figure 4.7. The dashed line corresponds to the critical κ for the flag of constant length L_0 , while the solid line corresponds to that of the flag of varying length L . The equation slightly overestimates the value of κ_{lower} that was experimentally observed, including the case of a single flag, presumably due to small variations in flow uniformity and initial curvature.

For $\frac{L}{L_0} < 1$, the flag of length L_0 reaches its flapping range at lower flow speeds than the flag of length L . As is evident in figure 4.7, despite the fact that the flag of length L is under its critical κ , synchronization, mostly in an anti-phase mode, still occurs. The flag of length L was observed to flap in these conditions (figure 4.8a), implying that the motion and resulting vortex street of the longer flag is inducing a flapping motion in the shorter flag. For the opposite case, $\frac{L}{L_0} > 1$, a similar behavior was observed: synchronization occurs for wind speeds at which the flag of length L has reached its flapping regime but that of length L_0 has not. In this case, however, the shorter flag does not flap, but oscillates with small amplitude (figure 4.8b). These

oscillations are in phase with the flapping motion of the longer flag and are larger than the oscillations that occur when the flags move uncoupled (figure 4.8c). This leads to the conclusion that it is the flow displaced by the flapping flag that impinges on the short flag and causes it to deflect. These two different behaviors (induced flapping and induced oscillations) in a seemingly symmetric problem arise because the distance between flags was maintained at a constant value and, therefore, the relative distance T/L is different in the two cases, with the flags being effectively closer in the $\frac{L}{L_0} > 1$ case.

4.2 Conclusions

This study has experimentally investigated the interaction between two inverted flags that are placed side-by-side in a uniform flow and the resulting coupled motion in the flapping and deflected regimes. It is relevant to the analysis of natural phenomena, such as leaves flapping in the wind, where multiple flags are generally present, as well as to the design of energy harvesting mechanisms, where the arrangement of multiple flags could be exploited to increase energy extraction.

Flags that were placed side-by-side saw an increase in flapping angular amplitude of up to 36% and an increase in frequency of up to 13% with respect to the motion of a single flag. Five different coupled modes of motion were observed in the flapping regime: in-phase, anti-phase, staggered, alternating and decoupled. The anti-phase mode is energetically favorable and predominant for small separations and low wind speeds, while the remaining modes appear for larger separations and high wind speeds. Inside, outside and asymmetric configurations are present in the deflected regime, with the inside configuration being the only one that presents a coupled in-phase motion.

Coupling was observed to occur between flags that had different lengths. However, the range of velocities at which coupling occurred was observed to diminish as the difference in flag lengths increased, with no coupling occurring for differences larger than 15%. Interestingly, the longer flag was observed to induce flapping on the shorter flag when the latter was outside of its flapping range.

A posterior experimental and theoretical analysis has been performed by Kim and Kim (2019) on side-by-side inverted flags at flag distances smaller than those presented in this chapter, complementing these results. For those distances and in the straight regime, Kim and Kim (2019) found that the gap flow pushes the flags to an out-of-phase outwards deflected equilibrium. This causes the flags to lose stability

at wind speed values lower than those of a single flag, with the critical wind speed increasing monotonically as the flag distance increases. At wind speeds between this lower critical value and the critical wind speed of a single inverted flag the flapping amplitude was, however, significantly smaller. In addition to the modes introduced here, Kim and Kim (2019) showed the existence of a static attached mode, where the leading edge of both flags is in contact.

An additional computational study of the side-by-side inverted-flag configuration has been implemented by Ryu et al. (2018). Their results show similar modes of motion as described above. Notably, when initialized in an in-phase mode, the flag motion remained in phase for a much wider range of parameters than found in this work. This may be explained by the much lower level of the perturbations present in the numerical framework compared to the experiments, that results in the flag not being perturbed away from the less energetically favorable in-phase mode. Finally, an interesting computational investigation of inverted flags in tandem and staggered configurations is presented in Huang et al. (2018). The readers are referred to the text for further information and details.